

TOWARDS ANALYTICAL MODELLING OF COMPRESSION-AFTER-IMPACT STRENGTH

Anton Köllner¹

¹ Technische Universität Berlin, Institute of Mechanics, Stability and Failure of Functionally Optimized Structures Group,
email: anton.koellner@tu-berlin.de,
website: <https://www.tu.berlin/en/svfs/about-us/team/dr-ing-anton-koellner>

Keywords: Delamination buckling, Compression-after-impact, Barely visible impact damage, Damage tolerance, Analytical modelling

ABSTRACT

Two analytical modelling approaches for determining nonlinear buckling responses of damaged composite panels are presented. The models consider localized delamination growth and nonlinear buckling responses during damage growth and thus extend current capabilities of analytical models for predicting the compression-after-impact strength of composite laminates. Modelling localized delamination growth is facilitated by employing a problem description in cylindrical coordinates with the energy release rate being analysed along the delamination boundary with the aid of an analytical crack-tip element. Nonlinear buckling responses during damage propagation are modelled by employing a so-called extended total potential energy. Predictions of both models are in good agreement with more exacting finite element analyses and corresponding experimental tests. The models outline a path towards developing (semi-)analytical models that may be used for designing damage tolerant composite structures.

1 INTRODUCTION

Damage tolerance is a major design driver for aerospace composite laminates. Structures are designed to withstand design ultimate loads in the presence of so-called barely visible impact damage (BVID). BVID comprises delamination damage alongside matrix cracks and possibly fibre fracture. The effect of BVID on the laminate strength is most pronounced for compressive in-plane loading, which is a characteristic load case in designing damage tolerant composite structures within the aerospace industry, i.e. compression-after-impact (CAI) loading [1]. Predicting the CAI behaviour and strength is utmost challenging and requires high-fidelity numerical models [2]. Owing to their enormous computational cost, although practically useful, such models are not suitable for design practice and also impede some fundamental insight into the interplay of delamination buckling with various failure mechanisms [3]. However, available (semi-)analytical models do not capture the complexity of the associated deformation processes in enough detail to predict CAI strength reliably and provide detailed understanding of the crucial failure mechanisms in CAI loading; and, thus, do not offer themselves as damage tolerant design models. Given the complexity and associated uncertainty regarding the structural response towards attaining its ultimate strength, the current certification requirement in the aerospace industry is that BVID should not grow under limit (once in a lifetime) load conditions [4]. Strength limits are determined by coupon testing of laminates containing BVID, which does not allow for new design concepts and highlights the need for analytical models capable of predicting the compressive strength of such laminates, which has yet to be accomplished. Considering that the main damage inducing failure mechanism of CAI loading scenarios is buckling-driven propagation of delaminations, analytical models capturing sufficient features of this failure mechanism will constitute a significant advance of the current state-of-the-art.

In this context, the current work resolves two key issues that impede the applicability of current analytical models. First, localized delamination growth is accounted for predicting the onset of delamination propagation. Second, nonlinear buckling responses beyond the initiation of damage growth are considered. Both characteristics are incorporated in (semi-)analytical modelling approaches [5–7]

that facilitate efficient predictions of the initiation of buckling-driven delamination growth and the study of the interactions between delamination buckling and failure mechanisms. The models advance the state-of-the-art towards analytical modelling of CAI strengths of composite laminates.

2 MODELS

2.1 Model I – Damage allowable strains

Model I considers buckling-driven delamination propagation which is the main failure mechanism in CAI loading. Currently, it is assumed that delamination damage can be represented by a single circular delamination with the respective sublaminates having constant thickness. The geometric model of a composite plate with an embedded circular delamination is shown in Fig. 1. The plate can be regarded as a semi-infinite plate where loading is applied in the form of far-field compressive strains, ε_0^x and ε_0^y , respectively, directed along respective Cartesian coordinate axes (x , y). The current modelling approach considers delaminations that are within the range associated with thin-film delaminations ($a \leq 0.1$), thus local buckling responses of the sublaminates (part 1 in Fig. 1) are modelled.

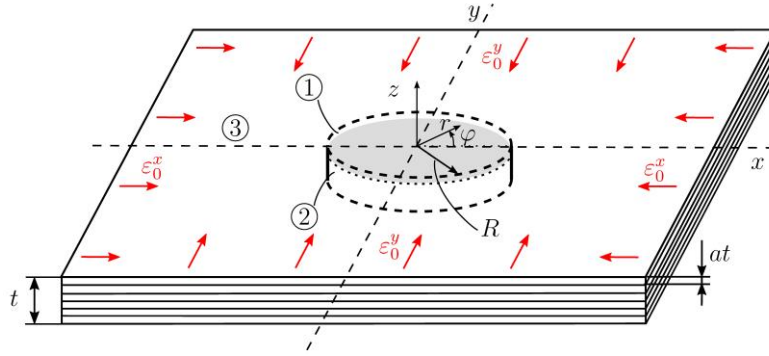


Figure 1: Geometric model of a composite plate with a circular delamination.

The problem is formulated using cylindrical coordinates (r , φ , z). This is deemed beneficial regarding the representation of the displacement field in terms of radially symmetric and asymmetric shape functions as well as the direct analysis and evaluation of the energy release rate along the delamination boundary. The Rayleigh–Ritz method is employed to determine nonlinear buckling responses; trigonometric series are used to approximate the displacement field, thus:

$$u(r, \varphi) = [\varepsilon_0^x r \cos^2(\varphi) + \varepsilon_0^y r \sin^2(\varphi)] + \sum_{m=1}^{M^u} \sum_{n=0}^{N^u} \sin\left(\frac{m\pi r}{R}\right) [a_{mn}^u \sin(2n\varphi) + b_{mn}^u \cos(2n\varphi)], \quad (1)$$

$$v(r, \varphi) = [-\varepsilon_0^x r \cos(\varphi) \sin(\varphi) + \varepsilon_0^y r \cos(\varphi) \sin(\varphi)] + \sum_{m=1}^{M^v} \sum_{n=1}^{N^v} \sin\left(\frac{m\pi r}{R}\right) [a_{mn}^v \sin(2n\varphi) + b_{mn}^v \cos(2n\varphi)], \quad (2)$$

$$w(r, \varphi) = \sum_{m=1}^{M^w} \sum_{n=1}^{N^w} c_{mn}^w \cos\left(\frac{(2m-1)\pi r}{2R}\right) \cos\left(\frac{(2n-1)\pi r}{2R}\right) + \sum_{m=1}^{M_2^w} \sum_{m=1}^{N_2^w} \sum_{o=1}^{O^w} \sin\left(\frac{m\pi r}{R}\right) \sin\left(\frac{n\pi r}{R}\right) [a_{mno}^w \sin(2o\varphi) + b_{mno}^w \cos(2o\varphi)], \quad (3)$$

where u , v and w describe the radial, circumferential and out-of-plane displacements respectively. The

parameters $a_{ij}^{u,v}$, $b_{ij}^{u,v}$, c_{ij}^w and $a_{ij,k}^w$, $b_{ij,k}^w$ are sets of generalized coordinates that are subsequently comprised within a single set q_i . Under uniaxial loading (along the x -direction, see Fig. 1), the transverse extension of the parent laminate is considered by $\varepsilon_0^y = -\nu_{12}^{\text{par}} \varepsilon_0^x$, with ν_{12}^{par} being the major Poisson's ratio of the parent laminate.

The strain energy of the sublaminates (W_s) is calculated by

$$W_s = \frac{1}{2} \int_{\varphi} \int_r \varepsilon_I^0 A_{IJ} \varepsilon_J^0 + 2\varepsilon_I^0 B_{IJ} \kappa_J + \kappa_I D_{IJ} \kappa_J r dr d\varphi, \quad (4)$$

with the in-plane strains (ε_I^0) and curvatures (κ_I) being

$$\varepsilon_I^0 = \begin{pmatrix} \frac{\partial u}{\partial r} + \frac{1}{2} \left(\frac{\partial w}{\partial r} \right)^2 \\ \frac{1}{r} \frac{\partial v}{\partial \varphi} + \frac{u}{r} + \frac{1}{2} \left(\frac{1}{r} \frac{\partial w}{\partial \varphi} \right)^2 \\ \frac{1}{r} \frac{\partial u}{\partial \varphi} + \frac{\partial v}{\partial r} - \frac{v}{r} + \frac{1}{r} \frac{\partial w}{\partial r} \frac{\partial w}{\partial \varphi} \end{pmatrix}, \text{ and } \kappa_I = \begin{pmatrix} -\frac{\partial^2 w}{\partial r^2} \\ -\frac{1}{r^2} \frac{\partial^2 w}{\partial \varphi^2} - \frac{1}{r} \frac{\partial w}{\partial r} \\ -\frac{2}{r} \frac{\partial^2 w}{\partial r \partial \varphi} + \frac{2}{r^2} \frac{\partial w}{\partial \varphi} \end{pmatrix} \text{ respectively.} \quad (5)$$

Note that owing to the description in cylindrical coordinates the in-plane (A_{IJ}), coupling (B_{IJ}) and bending (D_{IJ}) stiffness matrices exhibit a dependency on the angle φ . However, with the aid of algebraic manipulations, the strain energy W_s (Eq. (4)) can be determined analytically for arbitrary stacking sequences, thus: $W_s = W_s(q_i, \varepsilon_0^x, \varepsilon_0^y, E_{11}, E_{22}, G_{12}, \nu_{12}, t_{\text{ply}}, R, \theta_n)$, where besides the material parameters, the fibre orientations of all n layers in the sublaminates (θ_n) as well as the radius (R) and ply thickness (t_{ply}) are provided symbolically, making the energy expression ideally suited for conducting parametric studies.

Contact between the sublaminates and the base laminate is considered by introducing constraint conditions on the buckling displacement at pre-defined control points p_m , thus augmenting the strain energy by terms $W_p = \sum_m^M q_m^p (w(p_m) - (c_m^p)^2)$ for M control points, where q_m^p are Lagrange multipliers representing the contact forces and c_m^p is a measure representing the offset between sublaminates and base laminate [5]. Nonlinear buckling responses are determined by solving the set of nonlinear algebraic equations $\partial W / \partial q_i = 0$, with $W = W_s + W_p$ and the parameters q_m^p and c_m^p being added to q_i .

With the nonlinear buckling response determined, the energy release rate (ERR) is calculated with the aid of a crack-tip element, as proposed in [8]. The formalism is adapted to the current problem description in cylindrical coordinates, which is described in detail in [5]. Following the virtual crack closure technique, the total ERR G can be determined by

$$G = \frac{1}{2} [c_{11}(n_{\text{ct}}^r)^2 + c_{22}(m_{\text{ct}})^2 + c_{33}(n_{\text{ct}}^\varphi)^2 + 2c_{12}n_{\text{ct}}^r m_{\text{ct}} + 2c_{13}n_{\text{ct}}^r n_{\text{ct}}^\varphi + 2c_{23}n_{\text{ct}}^\varphi m_{\text{ct}}], \quad (6)$$

where n_{ct}^r and n_{ct}^φ are the crack-tip forces in radial and circumferential directions, respectively, and m_{ct} is the crack-tip moment. The parameters c_{ij} (provided in [5]) comprise compliances of the sublaminates and the base laminate as well as respective thickness measures. Mode I and mode II contributions of the ERR can be obtained following the non-standard mode separation as described in [9], thus:

$$G_{\text{I}} = \frac{1}{2} [-\sqrt{c_{11}}n_{\text{ct}}^r \sin(\Omega) + \sqrt{c_{22}}m_{\text{ct}} \cos(\Omega + \Gamma)]^2, \quad (7)$$

$$G_{\text{II}} = \frac{1}{2} [\sqrt{c_{11}}n_{\text{ct}}^r \cos(\Omega) + \sqrt{c_{22}}m_{\text{ct}} \sin(\Omega + \Gamma)]^2, \quad (8)$$

with $\Gamma = \sin^{-1}[c_{12}(c_{11}c_{22})^{-1/2}]$, where mode III contributions are determined by $G_{\text{III}} = G - G_{\text{I}} - G_{\text{II}}$. The mode-mix parameter depends only on the delamination depth and remains constant for thin-film

configuration at 24° [5, 9]. The ERR is monitored along the deformation path for each equilibrium state determined. The critical energy release rate G_c is calculated using the B-K-fracture criterion [10].

2.2 Model II – Nonlinear buckling responses considering damage propagation

Model II addresses the issue of describing nonlinear buckling responses beyond the deformation state associated with the onset of damage propagation, e.g. the initiation of delamination growth, which may have significant effects on the load carrying capacity of composite structures. The model employs a novel analytical framework presented in [7]. Fig. 2 shows the geometric model of a damaged composite plate strip loaded under uniaxial compression. Multiple damage mechanisms comprising two delaminations (see L_1 and L_2) and matrix cracked layers are considered. The depths of the delaminations are characterized by the parameters a_1 and a_2 , respectively. Matrix cracks are characterized by a matrix crack density D_{mc} being the ratio of the ply thickness to half the distance between two matrix cracks. The matrix cracks are assumed to be evenly distributed within the area of the delaminations.

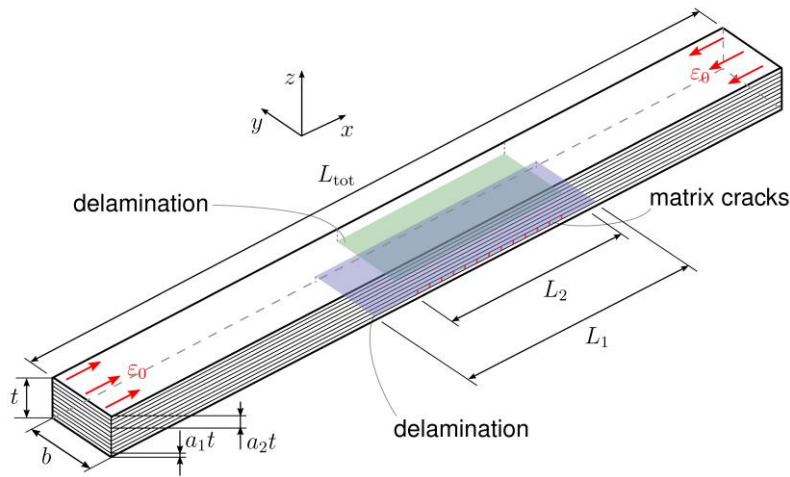


Figure 2: Geometric model of a composite plate with a circular delamination.

The in-plane (A_{IJ}), coupling (B_{IJ}) and bending (D_{IJ}) stiffness entries for the matrix cracked regions are determined with the aid of the Equivalent Constrained Model (see [11]). A one-dimensional problem description is employed, where the plate strip is subdivided into five regions as illustrated in Fig. 3 also highlighting exemplarily damage parameters entering the problem formulation.

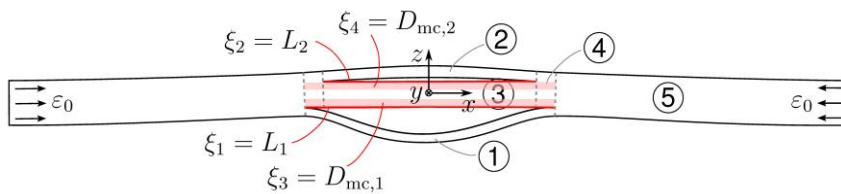


Figure 3: Sketch showing all regions of the plate strip as well as damage parameters.

A Rayleigh-Ritz formulation is employed. For each region, the out-of-plane displacement $w(x)$ is approximated with the buckling expression of the clamped-clamped Euler case employing the coordinate system shown in Fig. 3. The in-plane displacement $u(x)$ of each region is approximated by a sine series where contributions from rotations of the delaminated regions are considered (see [7]). The strain energy of the plate strip comprises the strain energies of each region, thus $W_s = \sum_{n=1}^5 W_s^{(n)}$, with

$$W_s^{(n)} = \frac{1}{2} b \int_x A_{11}^{\text{eff}(n)} \left(\varepsilon_{xx,0}^{(n)} \right)^2 + 2B_{11}^{\text{eff}(n)} \varepsilon_{xx,0}^{(n)} \kappa_{xx}^{(n)} + D_{11}^{\text{eff}(n)} \left(\kappa_{xx}^{(n)} \right)^2 dx \quad (9)$$

and is determined analytically, i.e. $W_s = W_s(q_i, \varepsilon_0, A_{11}^{\text{eff}(n)}, B_{11}^{\text{eff}(n)}, D_{11}^{\text{eff}(n)}, L_1, L_2, D_{\text{mc}}^j)$. As described for Model I, contact conditions are enforced. The delamination lengths and the j matrix crack densities represent the damage parameters of the given problem, summarized in the set ξ_k . Following the framework presented in [7], all damage parameters are described by functions of the structural configuration (in terms of the generalized coordinates q_i) and the applied loading (ε_0), thus: $\xi_k = \xi_k(q_i, \varepsilon_0)$, by exploiting the equality between thermodynamic forces (crack/damage driving forces) and corresponding material thresholds that holds during stable damage propagation. It should be noted that closed form expressions of the damage parameters cannot be derived. However, Taylor series approximations around the deformation state causing damage growth can be readily obtained (see [7]). By replacing the damage parameters in the total energy expression of the system, an extended total potential energy Π^* can be derived, thus:

$$\Pi^*[q_i, \varepsilon_0, \xi_k(q_i, \varepsilon_0)] = W_s[q_i, \varepsilon_0, \xi_k(q_i, \varepsilon_0)] + \Phi[\xi_k(q_i, \varepsilon_0)], \quad (10)$$

where Φ is the dissipative energy associated with the k damage parameters and $\xi_k = \{L_1(q_i, \varepsilon_0), L_2(q_i, \varepsilon_0), D_{\text{mc}}^j(q_i, \varepsilon_0)\}$. Note that the energy terms associated with enforcing the contact conditions are omitted in Eq. (10). Nonlinear buckling responses during damage propagation are obtained by solving the set of nonlinear algebraic equations $\partial \Pi^* / \partial q_i = 0$. In the solution algorithm, it is expedient to use linear approximations of the damage parameters given that the step sizes employed are sufficiently small during damage propagation. It should be noted that the irreversibility condition of damage growth (2nd law of thermodynamics) is considered in the analytical framework (see [7]).

3 RESULTS

3.1 Damage allowable strains

Model I has been validated by comparisons against results from experimental tests, as documented in [6], as well as three-dimensional finite element (FE) analysis, see [5]. Quasiisotropic stacking sequences are considered. The material parameters of the unidirectional (UD) plies are provided in Table 1.

Material parameters	
E_{11}	128,0 GPa
E_{22}	10.3 GPa
G_{12}	6.0 GPa
ν_{12}	0.3
G_c^I	0.268 N/mm
G_c^{II}, G_c^{III}	0.738 N/mm

Table 1: Material parameters of UD plies used in Models I and II.

First, model predictions for three distinct types of sublaminates are compared against experimental data and FE simulations in Table 2, where the applied strain causing the initiation of delamination growth, i.e. threshold strains or damage allowable strains, is provided. In the experimental tests, this measure is determined with the aid of digital image correlation, see [6].

Sublaminates	Damage allowable / Threshold strains ε^{th} in $\mu\varepsilon$			
	Model predictions		FE results	Experiment
	G_c^I	G_c^{mix}		
[0/90/90//...]	3410	3960	3580	3870
[45/-45//...]	6020	7790	7280	7080
[0/45//...]	2990	3580	3310	2890

Table 2: Damage allowable strains; Model I, FE results and experiments (mean of three tests).

In Table 2, two threshold strains are provided for Model I corresponding to a pure mode I fracture criterion and a mixed mode criterion using the B-K-law. Very good agreement is documented for sublaminates [0/90/90] and [45/-45]. Sublaminates [0/45] exhibits the largest deviations with experiments, despite predictions of Model I and FE analysis showing good agreement. The capability of Model I to evaluate the ERR along the delamination boundary accurately is highlighted in Fig. 4 showing the normalized ERR (against G_c) for sublaminates [0/90/90] and [0/45]. Figure 4 shows very good agreement between Model I and FE analysis, where the direction of delamination growth as well as the general behaviour of the ERR along the boundary is accurately predicted.

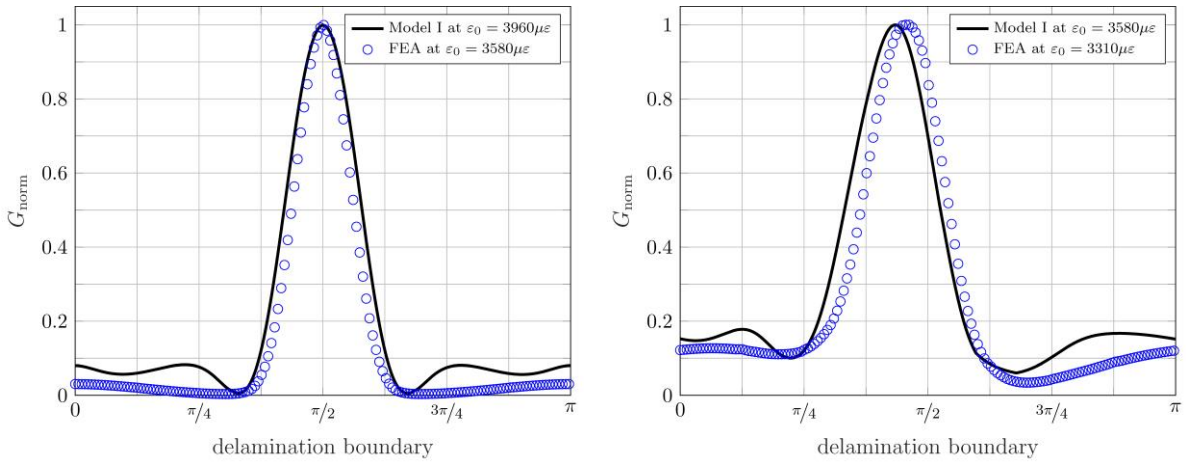


Figure 4: ERR along the delamination boundary at ε^{th} for (left) [0/90/90] and (right) [0/45].

Subsequently, a parametric study has been conducted. Considering quasiisotropic laminates, three types of sublaminates are considered:

- (i) stacking sequences exhibiting extension-twist/shear-bend coupling but no extension-shear and bend-twist coupling;
- (ii) stacking sequences with full mechanical coupling;
- (iii) stacking sequences exhibiting extension-shear and bend-twist coupling but with all coupling stiffness entries being zero.

Characteristic stacking sequences are selected for each type of sublaminates. For type (i), sublaminates with the stacking sequence [45/-45] and [45/0/-45] are considered. For type (ii), sublaminates [45/0] and [45/-45/0] are analysed. Type (iii) stacking sequences are represented by off-axis (multiple) unidirectional plies such as [45₂].

In Fig. 5, results are evaluated in the form of damage allowable (threshold) strain against the geometric parameter χ providing a ratio of delamination diameter to delamination thickness. As in Table 2, predictions for a mode I and a mixed-mode fracture criterion are considered. The results are compared against three-dimensional FE simulations employing solid elements in Abaqus (see [5]). For all types of stacking sequences and delamination sizes considered, FE results fall in between the predictions of the model. For type (i), damage allowable strain predictions of the model are in good agreement with FE results employing the mixed mode criterion, with deviations of roughly 10%.

Employing a mode I criterion for such stacking sequences represents a strong conservative lower bound for damage allowable strain predictions.

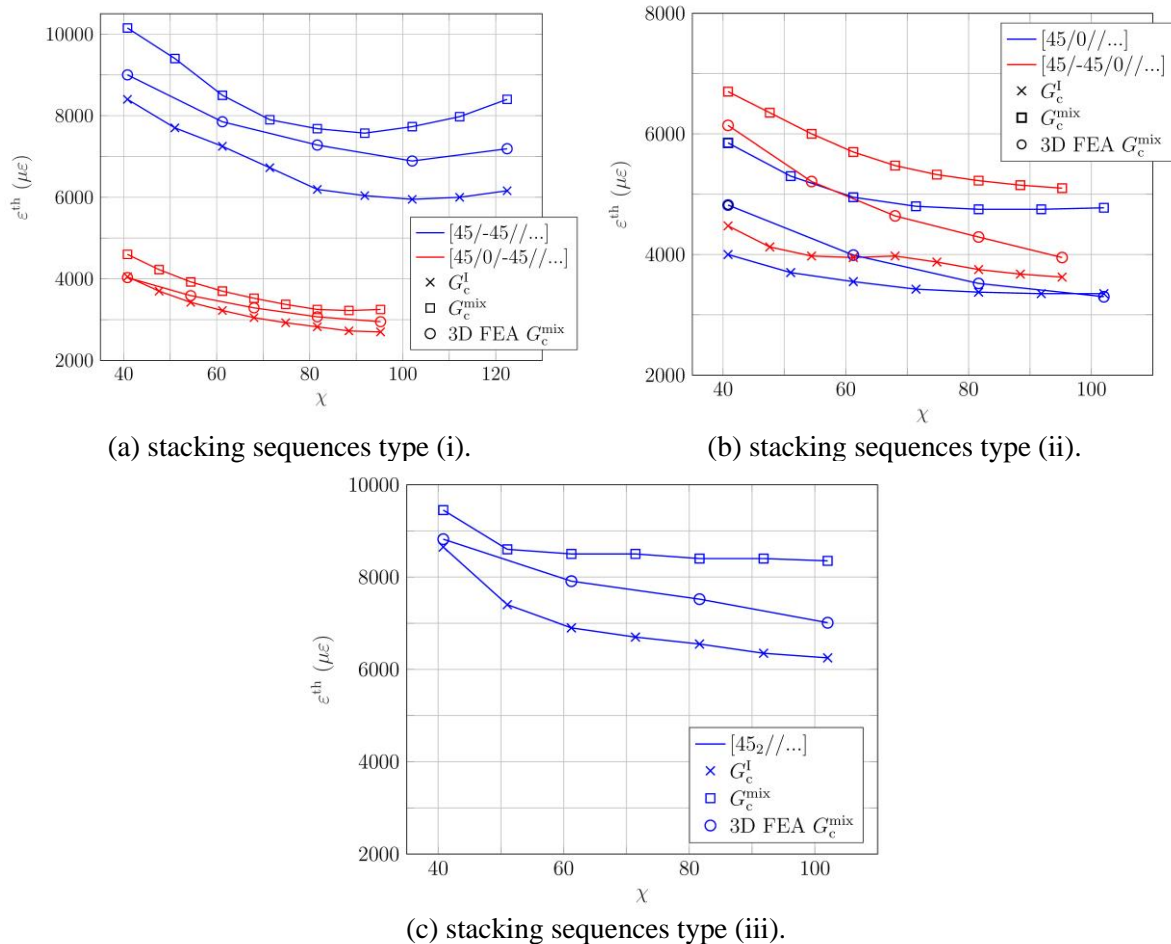


Figure 5: Damage allowable strains against delamination size.

As observed in Table 2, the largest deviations are present for type (ii) sublaminates with full mechanical coupling. As discussed in [5], such deviations are mainly associated with larger critical energy release rates determined by Model I than present in the FE analysis. This is related to discrepancies in determining mode I and mode II contributions of the ERR for such stacking sequences, where good agreement for the total ERR can be observed. It should be noted that for type (ii), mode I predictions of the model also provide a conservative lower bound for damage allowable strains. For type (iii), good agreement between the model and FE analysis is present, where, except for large delaminations, deviations are within 10%.

The results highlight that outer layers with a stacking sequences of [45/-45] appear to exhibit the largest damage allowable strains, which also holds when a third layer is part of the sublaminate. This can be seen by comparing stacking sequences [45/-45/0] with [45/0/-45] in Figs. 5a and 5b respectively. The effect of the stacking sequence on the damage allowable strains can also be highlighted by comparing the results for the sublaminate [45/0] with [0/45] from the experiments in Table 2 (the corresponding delamination size is $\chi \approx 100$).

3.2 Nonlinear buckling during damage propagation

In an exemplary study employing Model II, nonlinear buckling responses of a damaged composite plate strip with a cross-ply layup [(0/90)_s]₇ are analysed. The depths of the delaminations are taken as

$a_1 = 1/28$ (between the first and second layer) and $a_2 = 3/28$ (between the 25th and 26th layer), respectively (cf. Fig. 2). The material parameters of the UD plies are provided in Table 1. The length and width of the plate strip are taken as 200 mm and 10 mm respectively. The results of Model II are compared against geometrically nonlinear FE analyses employing the virtual crack closure technique to model delamination growth [7].

Two distinct nonlinear buckling responses can be observed by changing the initial length of the delaminations (L_1, L_2), which are subsequently referred to as type A and type B, respectively. The corresponding structural responses are provided in Fig. 6 in terms of load against end-shortening (Figs. 6a and 6c) and load against midpoint deflection of the sublaminates (Figs. 6b and 6d). Both types of post-buckling behaviour are characterized by delamination growth being the dominant damage mechanism triggered in the post-buckling regime (matrix crack growth is not initiated within the range considered in Fig. 6). Moreover, contact between sublaminates occurs for both types once global buckling of the parent laminate is triggered. Type A responses are characterized by a limit point behaviour once delamination growth is caused (Figs. 6a and 6b). Restabilization of the post-buckling response at larger end-shortening can be observed with subsequent stable delamination growth. Contrary, type B responses are characterized by delamination growth that barely affects the post-buckling behaviour, thus the post-buckling behaviour remains initially stable during delamination growth. However, unstable delamination growth, thus catastrophic failure of the plate strip is suddenly caused at later stages in the post-buckling range, which can be associated with the initiation of delamination growth of the second delamination (L_2), as documented in Figs. 6c and 6d.

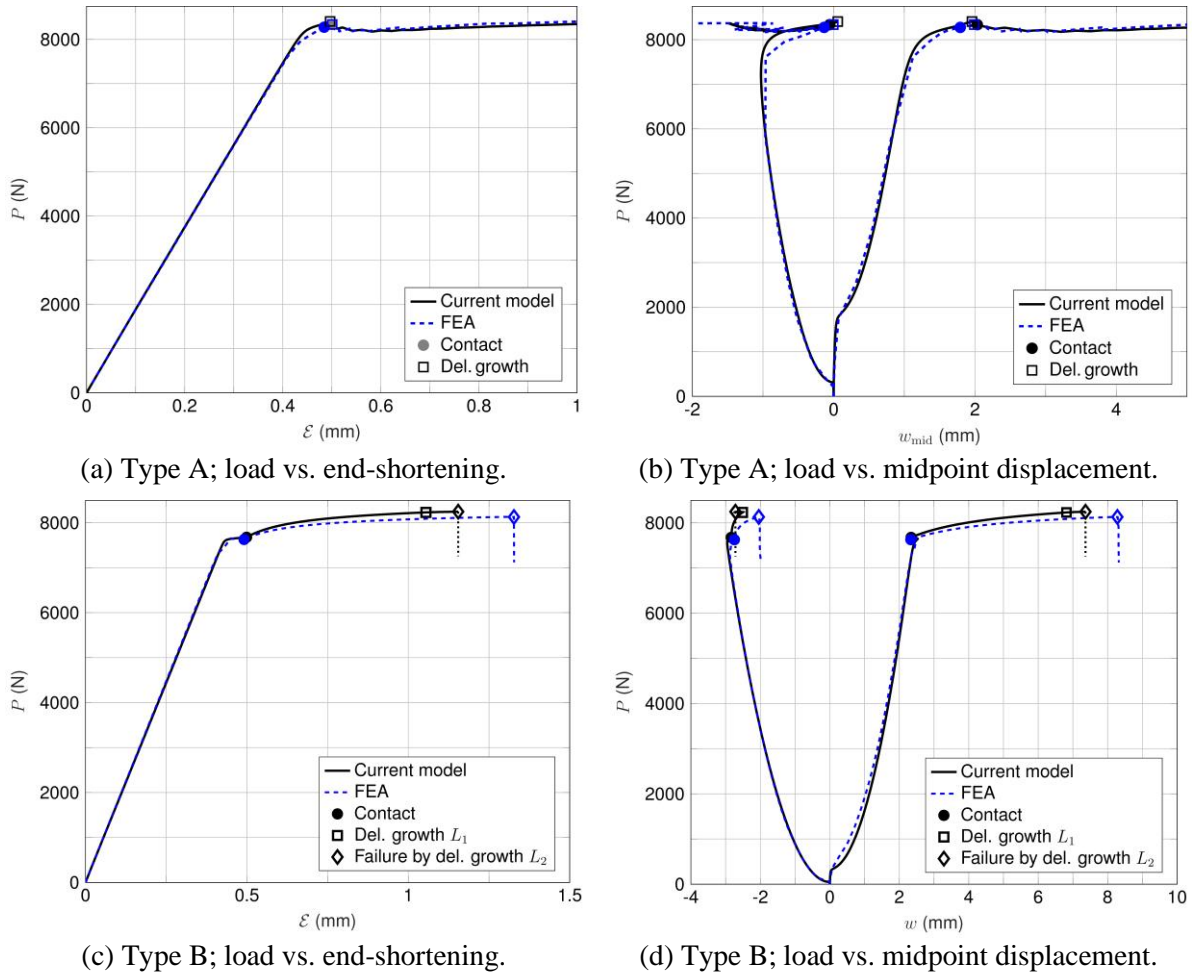


Figure 6: Nonlinear buckling responses with damage growth; type A: initial delamination lengths: $L_1 = 39$ mm, $L_2 = 35$ mm; type B: initial delamination lengths: $L_1 = 98$ mm, $L_2 = 78$ mm.

4 CONCLUSIONS

Two analytical modelling approaches have been presented which address some issues that currently impede the applicability of analytical models for laminate strength predictions of composites with BVID within the context of designing damage tolerant composite structures. The models accurately determine damage allowable strains and nonlinear buckling responses during delamination growth for idealized configurations of damage. Damage allowable strains that are in good agreement with more exacting FE analyses and experimental data have been obtained by considering a precise description of the post-buckling deformation, full mechanical coupling, mode-mixity and an evaluation of the ERR along the delamination boundary and thus localized delamination growth. It should be noted that the idealized damage configuration does not represent the actual damage morphology of BVID. However, the model provides the capability of studying in detail the dominant failure mechanism of composites with BVID loaded under in-plane compression, i.e. buckling-driven delamination growth, where relationships between damage allowable strains with stacking sequences and delamination sizes can be determined and analysed.

To determine the ultimate strength of damaged composite structures under in-plane compressive loading requires the modelling of nonlinear buckling responses that consider damage propagation. To date, such structural responses have solely been determined by means of purely numerical approaches (e.g. FE method). The model presented provides an approach to determine nonlinear buckling responses up to the ultimate strength by means of a semi-analytical approach. The approach is successfully applied to the problem of a composite plate strip exhibiting multiple damage mechanisms (delaminations and matrix cracked layers). Good agreement with FE analysis has been obtained. For employing the modelling approach to predict the ultimate strength of composite structures, extensions to two-dimensional problem descriptions alongside a more complex representations of BVID are required.

ACKNOWLEDGEMENTS

The author wants to thank the German Academic Exchange Service (DAAD) for the financial support to participate at the 23rd International Conference on Composite Materials (ICCM23).

REFERENCES

- [1] C. Kassapoglou, *Design and analysis of composite structures*, 2nd edition, John Wiley & Sons, 2013.
- [2] W. Tan, B.G. Falzon, L.N.S. Chiu and M. Price, Predicting low velocity impact damage and compression-after-impact (CAI) behaviour of composite laminates, *Composites Part A*, **104**, 2016, pp. 212–226.
- [3] J.-A. Pascoe, Slow-growth damage tolerance for fatigue after impact in FRP composites: why current research won't get us there, *Theoretical and Applied Fracture Mechanics*, **116**, 2021, 103127.
- [4] EASA, Certification specifications and acceptable means of compliance for large aeroplanes, 2013.
- [5] A. Köllner, Predicting buckling-driven delamination propagation in composite laminates: An analytical modelling approach, *Composite Structures*, **266**, 2021, 113776.
- [6] A. Köllner, M.W. Nielsen, J. Srisuriyachot, A.T. Rhead and R. Butler, Buckle-driven delamination models for laminate strength prediction and damage tolerant design, *Thin-Walled Structures*, **161**, 2021, 107468.
- [7] A. Köllner and A.W. Wadee, A novel discrete coordinate approach to modelling nonlinear structural instability problems with material damage, *European Journal of Mechanics / A Solids*, **96**, 2022, 104748.
- [8] B.D. Davidson, H. Hu and R.A. Schapery, An analytical crack-tip element for layered elastic structures, *Journal of Applied Mechanics ASME*, **62**, 1995, pp. 294–305.
- [9] B.D. Davidson, L. Yu and H. Hu, Determination of energy release rate and mode mix in three-dimensional layered structures using plate theory, *International Journal of Fracture*, **105**, 2000, pp. 81–104.

- [10] M.L. Benzeggagh, M. Kenane, Measurement of mixed-mode delamination fracture toughness of unidirectional glass epoxy composites with mixed-mode bending apparatus. *Composites Science and Technology*, **56**, 2013, pp. 439–449.
- [11] A. Köllner, M. Kashtalyan, I. Guz, C. Völlmecke, On the interaction of delamination buckling and damage growth in cross-ply laminates, *International Journal of Solids and Structures*, **120–121**, 2020, pp. 912–28.